Title

Targeted therapeutic nanotubes influence the viscoelasticity of cancer cells to overcome drug resistance.

Journal

ACS Nano, 8(5)

Authors

Bhirde, Ashwinkumar

Chikkaveeraiah, Bhaskara

Srivatsan, Avinash

et al.

Publication Date

2014-05-27

DOI

10.1021/nn501223q

Peer reviewed

Targeted Therapeutic Nanotubes Influence the Viscoelasticity of Cancer Cells to Overcome Drug Resistance

Ashwinkumar A. Bhirde,[†] Bhaskara V. Chikkaveeraiah,[†] Avinash Srivatsan,[†] Gang Niu,[†] Albert J. Jin,[‡] Ankur Kapoor,[§] Zhe Wang,[†] Sachin Patel,[∥] Vyomesh Patel,[∥] Alexander M. Gorbach,[‡] Richard D. Leapman,[‡] J. Silvio Gutkind,[∥] Angela R. Hight Walker,[⊥] and Xiaoyuan Chen[†,*]

[†]Laboratory of Molecular Imaging and Nanomedicine, National Institute of Biomedical Imaging and Bioengineering, National Institutes of Health, Bethesda, Maryland 20892, United States, [‡]Laboratory of Cellular Imaging and Macromolecular Biophysics, National Institute of Biomedical Imaging and Bioengineering, National Institutes of Health, Bethesda, Maryland 20982, United States, [§]Department of Radiology and Imaging Sciences, Clinical Center, National Institutes of Health, Bethesda, Maryland 20892, United States, [∥]Oral and Pharyngeal Cancer Branch, National Institute of Dental and Craniofacial Research, National Institutes of Health, Bethesda, Maryland 20892, United States, and [⊥]National Institute of Standards and Technology, Gaithersburg, Maryland 20899, United States

ABSTRACT Resistance to chemotherapy is the primary cause of treatment failure in over 90% of cancer patients in the clinic. Research in nanotechnology-based therapeutic alternatives has helped provide innovative and promising strategies to overcome multidrug resistance (MDR). By targeting CD44-overexpressing MDR cancer cells, we have developed in a single-step a self-assembled, self-targetable, therapeutic semiconducting single-walled carbon nanotube (sSWCNT) drug delivery system that can deliver chemotherapeutic agents to both drug-sensitive OVCAR8 and resistant OVCAR8/ADR cancer cells. The novel nanoformula with a cholanic acid-derivatized hyaluronic acid (CAHA) biopolymer wrapped around a sSWCNT and loaded with doxorubicin (DOX), CAHA-sSWCNT-DOX, is much more effective in killing drug-resistant cancer cells compared to the free DOX and phospholipid PEG (PL-PEG)-modified sSWCNT formula, PEG-sSWCNT-DOX. The CAHA-sSWCNT-DOX affects the viscoelastic property more than free DOX and PL-PEG-sSWCNT-DOX, which in turn allows more drug molecules to be internalized. Intravenous injection of CAHA-sSWCNT-DOX (12 mg/kg DOX equivalent) followed by 808 nm laser irradiation (1 W/cm^2, 90 s) led to complete tumor eradication in a subcutaneous OVCAR8/ADR drug-resistant xenograft model, while free DOX alone failed to delay tumor growth. Our newly developed CAHA-sSWCNT-DOX nanoformula, which delivers therapeutics and acts as a sensitizer to influence drug uptake and induce apoptosis with minimal resistance factor, provides a novel effective means of counteracting the phenomenon of multidrug resistance.

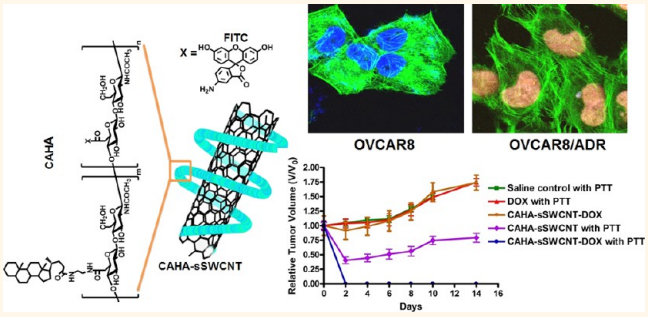

KEYWORDS: semiconducting carbon nanotube · hyaluronic acid · doxorubicin · multidrug resistance · viscoelasticity · live cell imaging · quartz-crystal microbalance with dissipation (QCM-D)

Multidrug resistance (MDR)[1] accounts for approximately 90% of chemotherapeutic drug failures in cancer patients.[2] These failures of chemotherapies, due to low tumor specificity, inadequate drug penetration to tumor site, and rapid clearance from circulation, lead to more intensive treatment regimens and debilitating side effects.[3,4] Nuclear-targeting chemotherapeutics such as doxorubicin (DOX) kill cancer cells by intercalating with DNA, which causes disruption in replication and ultimately apoptosis.[5,6] However, cells can become resistant to DOX owing to a complex MDR mechanism.[7] Lowering the resistance factor can help circumvent drug resistance. Recent studies have shown that combined chemotherapy and near-infrared (NIR) hyperthermia can help enhance drug uptake.[8] CD44 is a cell-surface glycoprotein that is involved in mediating cell−cell interactions, adhesion, and migration.[9] It is overexpressed in many solid tumors, thus making it a viable therapeutic target. Elevated levels of CD44 are also observed in drug-resistant cancer cells.[10−12] Thus, drug formulations that simultaneously target CD44 and deliver a payload of therapy may help overcome MDR and improve patient prognosis.[13,14]

* Address correspondence to (X. Chen) shawn.chen@nih.gov.

Received for review May 18, 2013 and accepted April 7, 2014.

Published online April 07, 2014
10.1021/nn501223q

Nanomaterials provide an innovative and promising alternative to conventional drug formulations for cancer therapies,[15−18] enabling efficient encapsulation, attachment, or covalent conjugation of drugs. It is expected that nanoformulas can improve delivery and stability *in vivo* and help circumvent many of the previously mentioned failings in conventional therapeutic approaches.[19−21] Through ligand-mediated receptor targeting,[22] these delivery systems are able to efficiently deliver the therapeutic payload to the tumor area and facilitate enhanced cellular uptake by the cancer cells.[23−25] Recently a DOX-loaded iron oxide nanodrug delivery system (nanoDDS) showed a quite low resistance factor against DOX-resistant cancer cells.[26] However, this and many other reported nanoDDSs involve multiple steps including fabrication of the nanoparticle core, adding a biocompatible layer, derivatization for functional groups, then adding a targeting moiety, and finally the drug loading step, with each step requiring purification, leading to a very low yield of the final nanoformula and inconvenience for scale-up synthesis. There is an urgent need for a simple yet effective targeted drug delivery system.

Carbon nanotubes[27−29] are a unique cylindrical nanomaterial with very high surface area (up to ~2600 m^2 g^{-1}) that have shown promise toward targeted therapies as drug delivery vehicles and photothermal therapy due to their strong optical absorption in the near-infrared biological window (0.7−1.4 μm),[30−32] but aggregation of nanotubes in aqueous media has added to the complexity in its formulation as an efficient nanoDDS.[33] A number of strategies (covalent/noncovalent modifications) have been used to render single-walled carbon nanotubes (SWCNTs) aqueous dispersible. However, a noncovalent approach is preferred over the covalent one, as it is noninvasive, thus preserving the inherent optical properties of the nanotubes.[34,35] Previously we have demonstrated that SWCNTs noncovalently modified with either phospholipid−poly(ethylene glycol) (PL-PEG) or cholanic acid−hyaluronic acid conjugate exhibited high stability *in vivo* and can be subjected to versatile chemical modification, such as arginine−glycine−aspartic acid (RGD) peptide to target integrin receptors and for high tumor accumulation or ^{64}Cu and Cy5.5 modification for PET and NIR fluorescence imaging.[36] To date, most reports of SWCNTs used in cancer therapy consist of heterogeneous mixtures of nanotubes, and only a small subset of chiral nanotubes can be effectively heated under a NIR laser. Semiconducting SWCNTs (sSWCNT) have shown tremendous potential for biomedical applications, and so far the focus has been on their biosensing capabilities.[37,38] Recently sSWCNTs have been reported to be highly aqueous stable and possess therapeutic value.[39−41] However, the therapeutic ability of sSWCNTs as drug delivery vehicles remains unexplored. Herein, we have engineered a novel nanoDDS that synergistically combines the optical properties of semiconducting therapeutic sSWCNTs and a multifunctional targetable biopolymer to address the challenge of drug delivery to MDR cancer cells.

Ovarian cancer is one of the leading causes of death globally from gynecological malignancies, with a 15−30% 5-year survival rate and MDR being the key factor in treatment failure and tumor reoccurrence.[42−44] CD44 is involved in cancer initiation and metastasis in ovarian cancer.[45,46] CD44 is also a natural receptor for hyaluronic acid.[47,48] In this study we utilized CD44 targeting cholanic acid-derivatized hyaluronic acid (CAHA) biopolymer[49,50] that self-assembled onto semiconducting SWCNTs in a single-step reaction to formulate a complete drug delivery system. The self-assembly resulted in very high recovery (over 80%, as compared to about 10% with commonly used PL-PEG coating material[51]) of the targetable therapeutic sSWCNT. This simple nanoDDS formulation allows high loading of clinically used chemotherapeutics such as DOX and behaves as a targeted nanoformula by specific delivery to CD44 receptor expressing tumor cells of a high payload of drugs. The newly developed nanoDDS is a sensitizer by acting as a NIR heat bomb for a photothermal therapy (PTT) agent[52−55] to enhance therapeutic efficacy against drug-resistant ovarian cancer cells. Viscoelastic responses of the drug-resistant cells treated with drug formulations indicated that targeted nanoformula is better than free drug or nontargeted sSWCNT. Our nanoDDS is effective in eradicating MDR tumors *in vivo* with a single dose of drug in combination with PTT. We believe viscoelastic features of drug-resistant cells in response to nanodrug delivery systems and free drug provide a new angle to explain why nanoformulas are highly successful in circumventing MDR, eventually delivering a high payload of drugs to the resistant cells with low resistance factor and its significance in the fight against MDR in cancer treatment.

RESULTS AND DISCUSSION

Therapeutic sSWCNTs were synthesized by a single-step reaction between sSWCNTs and CAHA similar to a previously reported protocol.[36] CAHA-sSWCNTs were 2−4 nm in diameter, as opposed to a core diameter of 0.7−0.9 nm before CAHA wrapping, with a length distribution of 0.2−2 μm. This process resulted in a high recovery of sSWCNTs (80%) with strong absorption peaks at 568 and 996 nm, indicative of (6,5) sSWCNTs (Figure 1A,B and Supplementary Figures S1 and S2).[56] The CAHA-sSWCNTs were characterized for structural morphology, purity (Raman spectroscopy), and optical absorption (Figure 1C−E and Supplementary Figure S3). Fluorescent probe tagging for intracellular tracking and surface charge analysis was performed (Figure 1F and Supplementary Figure S4).

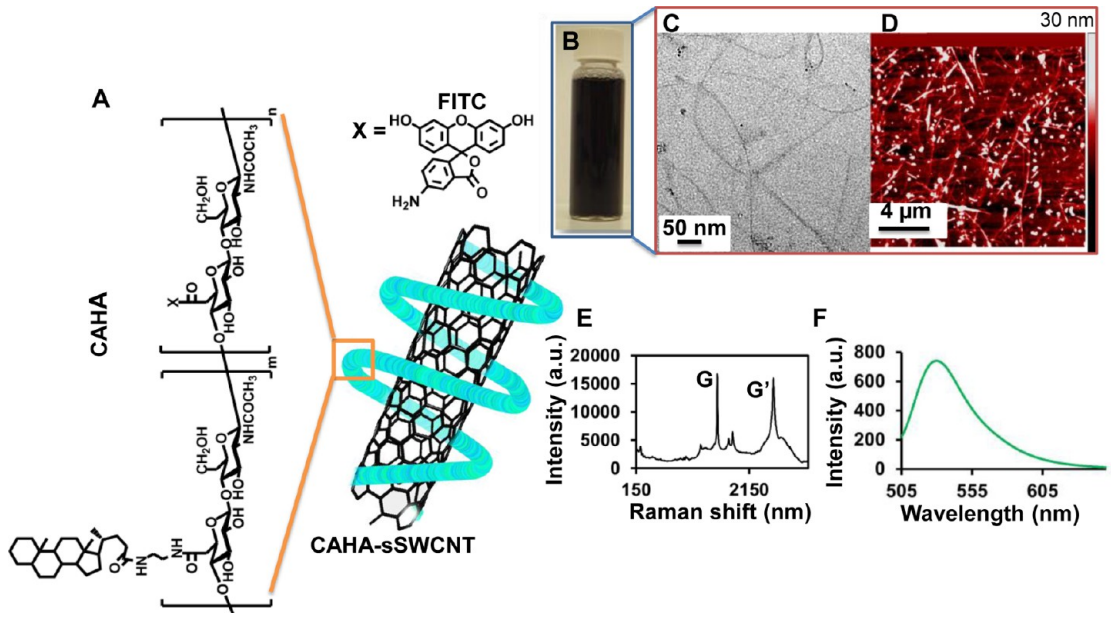

Figure 1. Self-assembled self-targetable multifunctional CAHA-sSWCNT nanodrug formulation. (A) Schematic showing cholanic acid-derivatized hyaluronic acid wrapped semiconducting SWCNTs (CAHA-sSWCNTs). (B) Photo of well-dispersed aqueous CAHA-sSWCNT dispersion. (C) Image of singly dispersed CAHA-sSWCNTs with a core size of ~1 nm. (D) AFM image of CAHA-sSWCNTs with a height of 2−4 nm, indicating successful CAHA wrapping of the sSWCNTs. (E) Raman analysis of CAHA-sSWCNTs showing the characteristic sSWCNT G and G′ bands at ~1600 and ~2600 nm, respectively. (F) Fluorescence spectrum of FITC-loaded CAHA-sSWCNTs showing a peak around 520 nm, indicating successful formation of green fluorescent CAHA-sSWCNTs.

Serum stability of the CAHA-dispersed sSWCNTs was tested in a unique near physiologically relevant setup using photon correlation spectroscopy (Supplementary Figures S5 and S6). CAHA-sSWCNTs were very stable without any aggregation over time by incubation with serum medium. The MTT assay showed that sSWCNTs after CAHA wrapping were not cytotoxic as a carrier (Supplementary Figure S7). Photothermal properties of CAHA-sSWCNTs were tested under the influence of a NIR laser probe at 808 nm wavelength for photothermal therapy. The nanotube dispersion (0.1 mg mL^{-1}) showed a rapid increase in temperature from 23 °C (RT) to 80 °C in just 120 s (808 nm laser power: 1 W/cm^2), suggesting high thermal capacity of the CAHA-sSWCNTs (Supplementary Figures S8 and S9). A CAHA-sSWCNT dispersion at a concentration as low as 5 μg/mL can still be heated to 50 °C in 2 min. The instant heat generation renders CAHA-sSWCNTs with the ability to kill drug-resistant cancer cells in addition to the DOX drug molecules loaded onto the surface of sSWCNTs.

Before moving on to drug delivery experiments we first tested the CD44-mediated selective uptake pathway of the FITC-tagged CAHA-sSWCNTs, which was confirmed using cells with varying levels of CD44 expression: SCC7 (low), NIH3T3 (negative), OVCAR8 (high), and OVCAR8/ADR (high) (Figure 2A). CD44-positive cells showed prominent while CD44-negative cells had almost negligible green fluorescence, confirming CD44-specific targeting of CAHA-sSWCNTs (Figure 2B). Next we would like to see if CD44 targeting improves cell uptake of DOX in drug-resistant cancer cells. After purification, CAHA-sSWCNT was tested for doxorubicin drug loading. Simple mixing of DOX with CAHA-sSWCNT resulted in high DOX loading efficiency due to combined $\pi-\pi$ stacking and encapsulation in the biopolymer (Figure 3A−C and Supplementary Figure S10). Both drug-sensitive OVCAR8 and -resistant OVCAR8/ADR cells were treated with either free DOX or DOX-loaded CAHA-wrapped sSWCNTs. DOX is also a fluorophore, and hence live fluorescence imaging in conjunction with a computational algorithm was used as readout of intracellular DOX uptake (Supplementary Figures S11 and S12). While DOX uptake was observed in both cell types, the accumulation patterns differed significantly. Free DOX failed to accumulate in the drug-resistant cells due to the presence of drug transporters,[57] while DOX delivered through CD44 targeting had strikingly high accumulation (Figure 4A−D). CD44-targeted drug delivery was further confirmed by the observation that minimal DOX uptake was observed for drug-resistant cells pretreated with CAHA before introducing CAHA-sSWCNT-DOX (Figure 4E). Figure 4F−J shows fixed cell fluorescence images of OVCAR8 and OVCAR8/ADR cells at the 4 h time point after being treated with free DOX or CAHA-sSWCNT-DOX. As expected, drug-sensitive cells treated with both free DOX and CAHA-sSWCNT-DOX resulted in nuclear localization of DOX. Although uptake of DOX was evident in the drug-sensitive cells, CAHA-sSWCNT-DOX showed faster diffusion (Figure 4K). Computational analysis of DOX

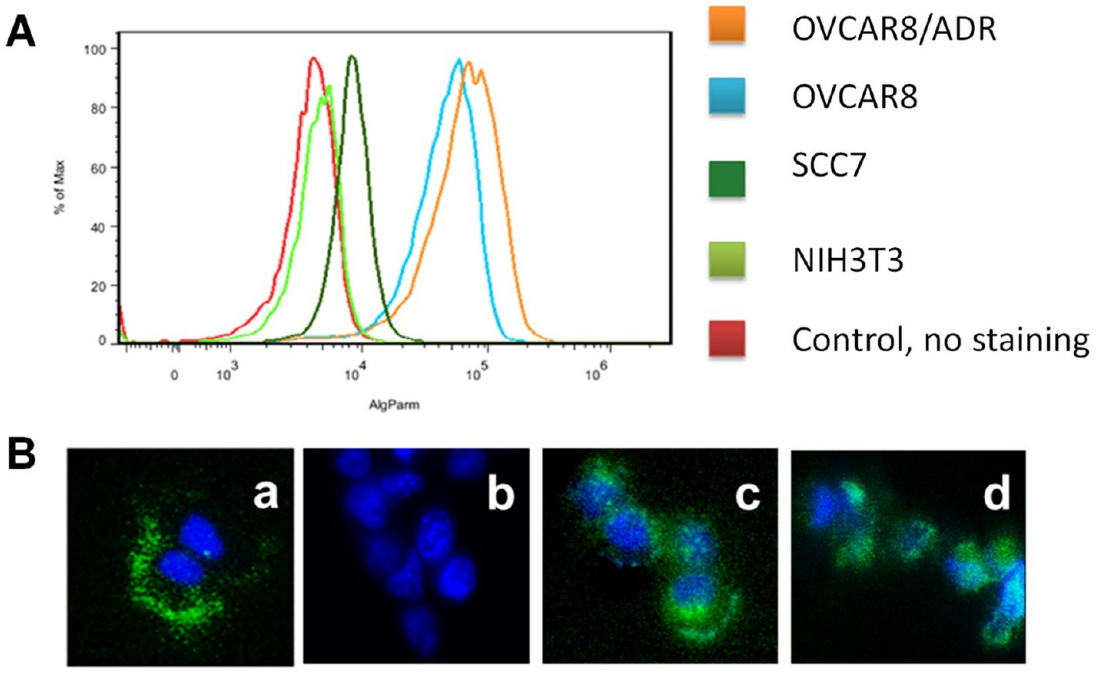

Figure 2. CD44-mediated cell uptake of CAHA-sSWCNTs. (A) FACS analysis shows that both OVCAR8 and OVCAR8/ADR ovarian cancer cell lines have a high expression of CD44 compared to SCC7 (CD44 low) and NIH3T3 (CD44 negative) controls. (B) CAHA-sSWCNT uptake in cells with varying levels of CD44 expression by fluorescence imaging of CAHA-sSWCNT-FITC (green) and nuclei stained with DAPI (blue): (a) SCC7 cells (CD44 low), (b) NIH3T3 cells (CD44 negative), (c) OVCAR8 cells (CD44 high), and (d) OVCAR8/ADR cells (CD44 high).

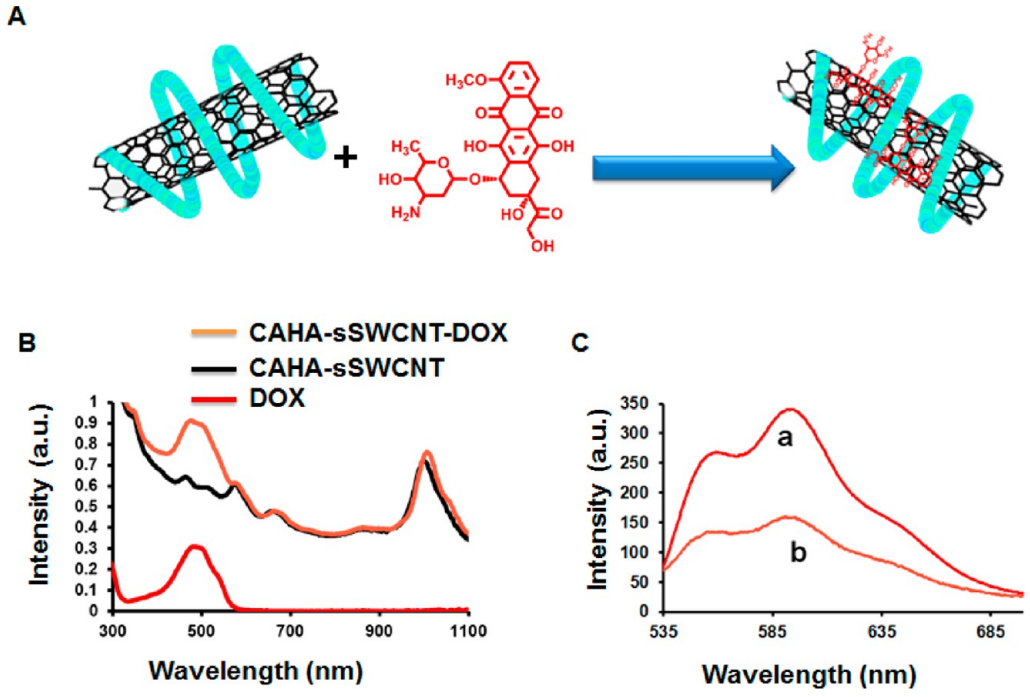

Figure 3. DOX loading onto CAHA-sSWCNTs. (A) Schematic showing the DOX loading onto CAHA-sSWCNTs through π stacking. (B) UV−vis absorbance spectra show efficient DOX loading (>300% w/w ratio) on the CAHA-sSWCNTs, where the red line is free DOX, the black line is CAHA-sSWCNTs only, and the orange line represents DOX-loaded CAHA-sSWCNTs. (C) Fluorescence spectra of free DOX (a) and CAHA-sSWCNT-DOX (b). DOX fluorescence was significantly quenched on the nanotube surface, although both samples had the same amount of DOX. This was also observed in earlier published studies.[64]

uptake in the resistant cells showed a very different pattern: free DOX had minimal uptake, while the nanoDDS formula facilitated much higher nuclear uptake of DOX over time (Figure 4L). DOX delivery to

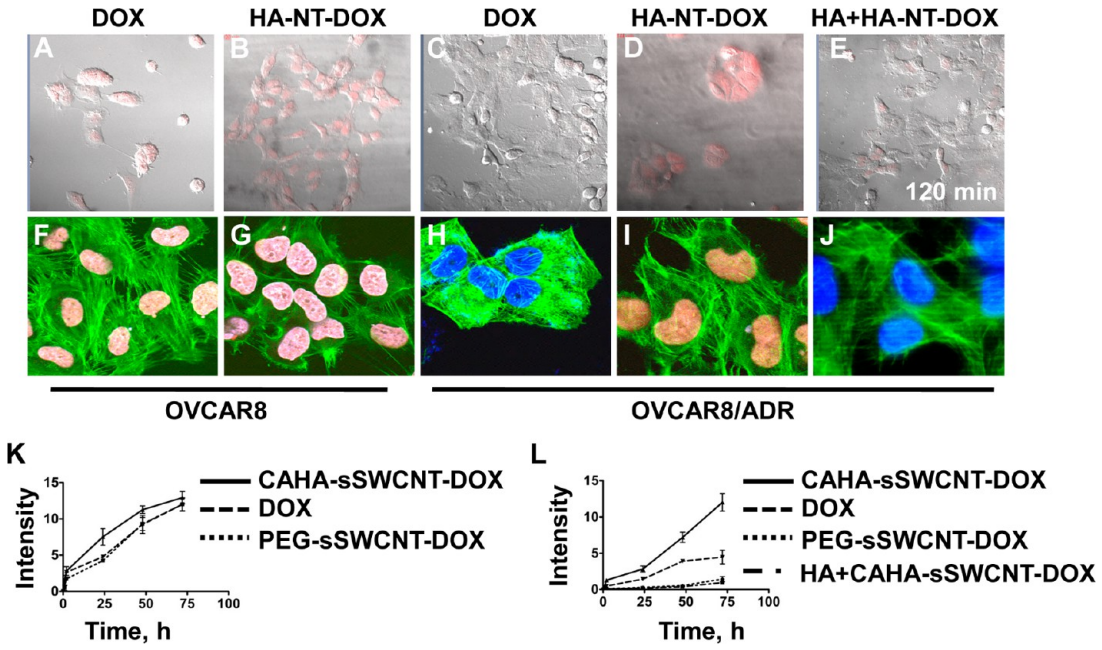

Figure 4. DOX uptake in DOX-sensitive OVCAR8 and DOX-resistant OVCAR8/ADR cells. (A−D) Snapshots of live cell confocal video imaging of DOX uptake in drug-sensitive (A, B) and -resistant (C, D) ovarian cancer cells at the 120 min time point, showing higher drug uptake with CAHA-sSWCNT-DOX. (E) OVCAR8/ADR cell uptake of CAHA-sSWCNT-DOX was effectively blocked in the presence of excess HA, suggesting CD44-mediated endocytosis of the nanoformula. (F−J) Fluorescence images of OVCAR8 (F, G) and OVCAR8/ADR cells (H, J), treated with free DOX or CAHA-sSWCNT-DOX for 4 h and fixed. Cell nuclei were stained with DAPI (blue) and cytoskeleton phalloidin with Alexa 488 (green). DOX is shown in red. (K, L) Plot shows the DOX intensity in OVCAR8 (K) and OVCAR8/ADR (L) cells treated with free DOX, PEG-sSWCNT-DOX, CAHA-sSWCNT-DOX, or HA + CAHA-sSWCNT-DOX at the 1, 2, 24, 48, and 72 h time points. Free DOX shows minimal uptake compared to CAHA-sSWCNT-DOX in both sensitive and resistant cancer cells at early time points, indicating that CAHA-sSWCNT-DOX can provide fast delivery of the drug molecules through CD44 targeting. CD44 blocking of resistant cells affects DOX uptake, which can be due to less internalization of the CAHA-sSWCNT carrier.

resistant cells through PEGylated phospholipid wrapped sSWCNTs (PEG-sSWCNT-DOX) was much less effective. Our data suggest that the CD44-targeted sSWCNT drug delivery system is desirable to counteract drug resistance to amplify drug accumulation similar to that of drug-sensitive cancer cells.

We successfully enhanced the uptake of drugs (DOX) in resistant cancer cells compared to free drugs or nontargeted nanoformula (PEG-sSWCNT-DOX) through an sSWCNT-based CD44-HA-mediated delivery system, although both drug-sensitive and -resistant cancer cells had similar levels of CD44 expression. We wanted to investigate why targeting CD44 leads to enhanced drug uptake. Here for the first time a quartz-crystal microbalance with dissipation (QCM-D) was utilized to look at the effect of the drug delivery system on drug-resistant cancer cells. The QCM-D is an acoustic wave sensor that measures changes in resonance frequency and energy dissipation when a layer of cells adhere to the sensor surface (Figure 5A). Here the resonator oscillates with some constant amount of energy, and as the amount of energy in the system remains constant, the oscillation frequency changes with addition of any mass onto the resonator surface. Changes in the amount of mass adsorbed are then measured through change in frequency (ΔF). ΔF does not always indicate a change in mass on the surface. Energy can be lost in other ways that would also change the frequency at which the sensor oscillates. This is measured by changes in dissipation (ΔD), which gives a qualitative measure of how rigidly the cell adheres to the underlying substrate. An increase in dissipation indicates more energy being lost to the surrounding environment, suggesting a relatively softer cell layer. Herein we noninvasively measured changes in resistant cancer cell viscoelasticity in real time and in a label-free manner through ΔF and ΔD.[58,59] We show that the ΔF and ΔD response reflects time-dependent changes in mechanotransduction and mechanical properties of the basal region of the cells caused by HA-CD44 interactions (Figure 5B, a−d). The differential multiphasic viscoelastic changes observed in drug-sensitive and -resistant cells toward CAHA-sSWCNT probes indicate that sSWCNTs are able to sneak through the membrane barriers encountered in a resistant cell more efficiently than the free ligand.

Biomechanical studies at the nanoscale suggest that different cancer cells have viscoelastic features.[60] In our QCM-D studies we found that among the cancer cells the viscoelastic properties and their response to CAHA and CAHA-sSWCNT treatment varied significantly between drug-resistant cancer cells and drug-sensitive cancer cells, as shown in the data plot (Figure 6). In the present study, the QCM-D was used to track the

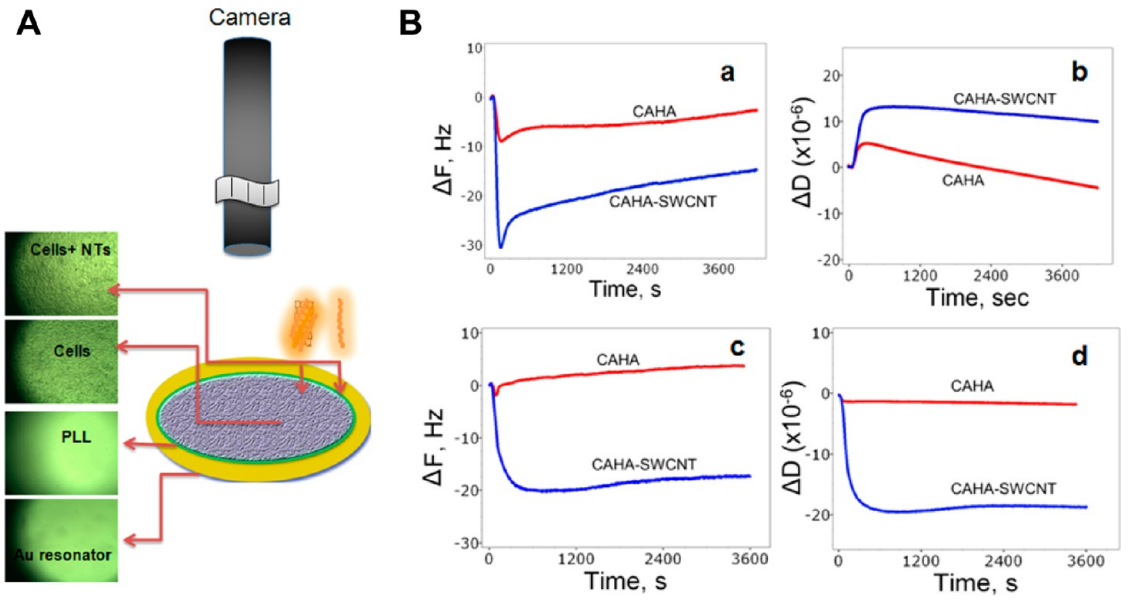

Figure 5. Assessment of viscoelastic behavior of cancer drug sensitive and resistant cells by a quartz-crystal microbalance with dissipation (QCM-D). (A) The QCM-D setup for investigating nanoformula−cancer cell interactions. Yellow is the bare Au-coated quartz-crystal resonator, green shows the polylysine layer added for efficient cell adhesion onto the Au resonators, and gray shows a monolayer of cells grown. A voltage is applied across the quartz crystal *via* electrodes. (B) Real-time frequency and dissipation plots of CAHA- and CAHA-SWCNT-treated OVCAR8 cells (a, b) and OVCAR8/ADR cells (c, d).

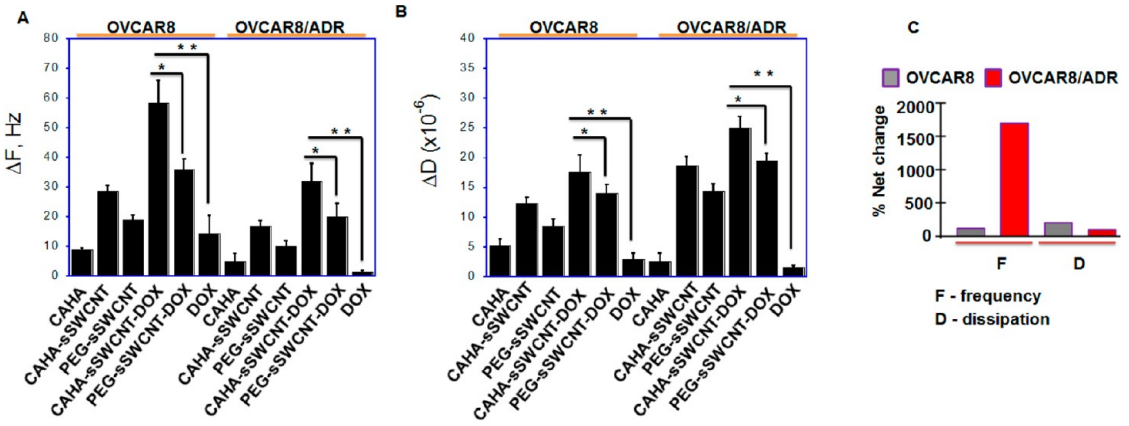

Figure 6. QCM-D analysis of therapeutic nanotubes on drug-sensitive and -resistant cancer cells. (A, B) Frequency and dissipation amplitude difference (A, ΔF; B, ΔD) are shown for CAHA (250 μg mL^{-1}), CAHA-sSWCNTs (5 μg mL^{-1} nanotube), PEG-sSWCNTs (5 μg mL^{-1} nanotube), CAHA-sSWCNT-DOX (2 μg mL^{-1} nanotube, 3 μM DOX), PEG-sSWCNT-DOX, and free DOX treated drug-sensitive OVCAR8 and drug-resistant OVCAR8/ADR cancer cells (n = 3 sensor-cell layers). Data show that CAHA-sSWCNT-DOX has a higher impact on the frequency and dissipation of sensitive and resistant cancer cells compared to the individual components of the nano drug delivery system. (C) Net change in frequency and dissipation for free DOX (D_1) to CAHA-sSWCNT-DOX (D_2) calculated using the formula $[((D_2 - D_1)/\lvert D_1\rvert) \times 100]$ with equivalent DOX concentration (1 μM).

short-term, CD44-mediated response of a confluent monolayer of ovarian OVCAR8 and OVCAR8/ADR cells. Stable baselines were achieved for all experiments prior to the addition of CAHA or CAHA-sSWCNTs (Supplementary Figure S13). Although the measurements were conducted at overtones n = 3, 5, 7, and higher, but results for all overtones echoed each other, only the results from n = 5 are presented. Both OVCAR8 and OVCAR8/ADR cells responded moderately to treatment with CAHA as free ligand or free DOX, with a negligible change in dissipation with drug-resistant cells, meaning the MDR cells remained rigid. However, the corresponding responses from CAHA-sSWCNT treatment are larger for both cell types (10−20 times). Especially, a significant change in dissipation was observed compared to free CAHA (Figure 6B and Supplementary Figure S14). The change in frequency due to mass change indicates a high uptake of CAHA-sSWCNTs compared to free HA. An increase in dissipation represents a decrease in viscoelasticity (rigidity), indicating that cells were getting softer, prompted by higher drug uptake. This is a significant new observation of viscoelastic behavior in drug-sensitive and -resistant cancer cells in response to a

nanoformula; however further in-depth study is required to fully elucidate this phenomenon. These results also show that acoustic wave sensors can be very informative when analyzing nanoformula interactions with drug-sensitive and -resistant cells by providing a label-free quantitative platform in real-time, noninvasively.

Killing of drug-resistant ovarian cells using the therapeutic nanotubes was assessed using the apoptotic cell death TUNEL assay and the live cell Calcein AM assay (Figure 7A,B). OVCAR/ADR cells were treated with free DOX, CAHA-sSWCNTs, or CAHA-sSWCNT-DOX for 6 h and then irradiated with a 808 nm laser at 0.5 W/cm^2 for 2.5 min. Cells were then fixed and analyzed for apoptosis. The apoptosis TUNEL assay (Figure 7A and Supplementary Figure S15) shows that cells treated with CAHA-sSWCNT-DOX and CAHA-sSWCNTs had positive staining for apoptosis, whereas free DOX and cells alone did not. The live cell Calcein AM assay (Figure 7B and Supplementary Figure S16) showed a similar trend in the reverse order, where cells with sSWCNTs showed fewer live cells compared to DOX or cells alone. Thr cell viability assay was carried out to assess the killing efficiency of nanoformulas (Figure 7C−F). Both OVCAR8 and OVCAR8/ADR cells were grown in 96-well plates and treated with CAHA, CAHA-sSWCNTs, free DOX, PEG-sSWCNT-DOX, or CAHA-sSWCNT-DOX overnight without or with 808 nm laser irradiation (1 W/cm^2 for 2.5 min). The MTT assay was carried out 48 h later. Throughout the experiment the nanoDDS formulation was prepared with equivalent DOX concentration for all the formulations being tested. The IC_{50} value of free DOX was 2.1 ± 1.7 μM without irradiation and 1.5 ± 2.3 μM with irradiation for OVCAR8 cells and was 150 ± 2.7 μM without irradiation and 99.8 ± 3.1 μM with irradiation for OVCAR/ADR cells. Without laser irradiation, the resistance factor (RF), ratio of respective IC_{50} values of drug-resistant and drug-sensitive cells, for free DOX was 71.4 ± 1.5 and that for CAHA-sSWCNT-DOX was 7.6 ± 0.8. With laser irradiation, the RF value was 66.5 ± 1.3 for free DOX and only 1.81 ± 1.0 for CAHA-sSWCNT-DOX, which is very significant in overcoming MDR. This is by far the lowest resistance factor ever reported by any nanodrug delivery system. For comparison, PEG-sSWCNT-DOX had an RF value of 12.1 ± 7.2 without laser irradiation and 6.9 ± 1.1 with laser irradiation.

With these encouraging results of overcoming MDR using therapeutic sSWCNTs we investigated the feasibility of using the targeted therapeutic CAHA-sSWCNT-DOX for *in vivo* PTT in an OVCAR8/ADR-resistant xenograft tumor model. Five groups of OVCAR8/ADR tumor-bearing mice (n = 6/group) were used for our experiment. At 24 h postinjection of CAHA-sSWCNT-DOX (12 mg/kg DOX equivalent), the mice were irradiated with an 808 nm laser for 90 s at a power density of 1 W/cm^2. Thermal imaging with an infrared thermal camera was used to follow tumor temperature increase. Following laser irradiation, the local tumor temperature reached about 73 °C (Figure 8A). No significant increase in temperature was observed in the rest of the body.

Groups administered CAHA-sSWCNT-DOX and CAHA-sSWCNT and subjected to laser irradiation showed a delay in tumor growth or complete tumor regression (Figure 8B and Supplementary Figure S17) (CAHA-sSWCNTs *vs* control, $p < 0.001$; CAHA-sSWCNT-DOX *vs* control, $p < 0.001$). All the other groups showed tumor recurrence and had to be euthanized by day 30 because of excessive tumor burden. The combination of doxorubicin and PTT allows for complete eradication of the drug-resistant tumors.

Biodistribution of the sSWCNT 24 h post-treatment was carried out using Raman spectroscopy, following the standard protocol previously established in our laboratories[61,62] (Figure 9A). Our nanoDDS on its own was nontoxic over the period of experiment, as there was no drop in the animal body weight (Figure 9B). To assess the *in vivo* biocompatibility, histology of the mice treated with nanoDDS was performed. Hematoxylin and eosin staining of the tumor slices as well as other organs was carried out following PTT treatment along with the control groups (Figure 10). There was significant damage in the tumor subjected to PTT treatment with the CAHA-sSWCNTs, but the other groups showed no adverse effects. All the other visceral organs also showed no damage, suggesting the biocompatibility of the CAHA-sSWCNTs. These results indicate that the CAHA-sSWCNTs are excellent agents for delivery as well as treatment of drug-resistant tumors. The interaction of endogenously available hyaluronic acid is important for tumor growth. It has been reported that disturbing this interaction might help in tumor reduction. The hyaluronic acid coating of the sSWCNTs might compete with the endogenously available HA, which exists in the tumor microenvironment. This blocking might cause a major disruption in the interactions of the tumor cells with its stroma, an important event for tumor growth and subsequent metastasis. We hypothesize that the HA coating, besides targeting the tumor, also prevents the interaction of the CAHA-sSWCNT formula with plasma proteins, thus increasing circulation time, and consequently the leaky vasculature of the tumor allows for increased uptake of the nanoparticles,[63,64] which explains the increased therapeutic efficacy of the drug-loaded nanoparticles.

CONCLUSION

Our study showed that a single dose of DOX delivered using targeted semiconducting single-walled carbon nanotubes along with PTT was able to completely eradicate OVCAR8/ADR MDR tumors *in vivo*. Cholanic acid-modified hyaluronic acid biopolymer wrapped sSWCNTs can act as self-targetable nanoprobes with

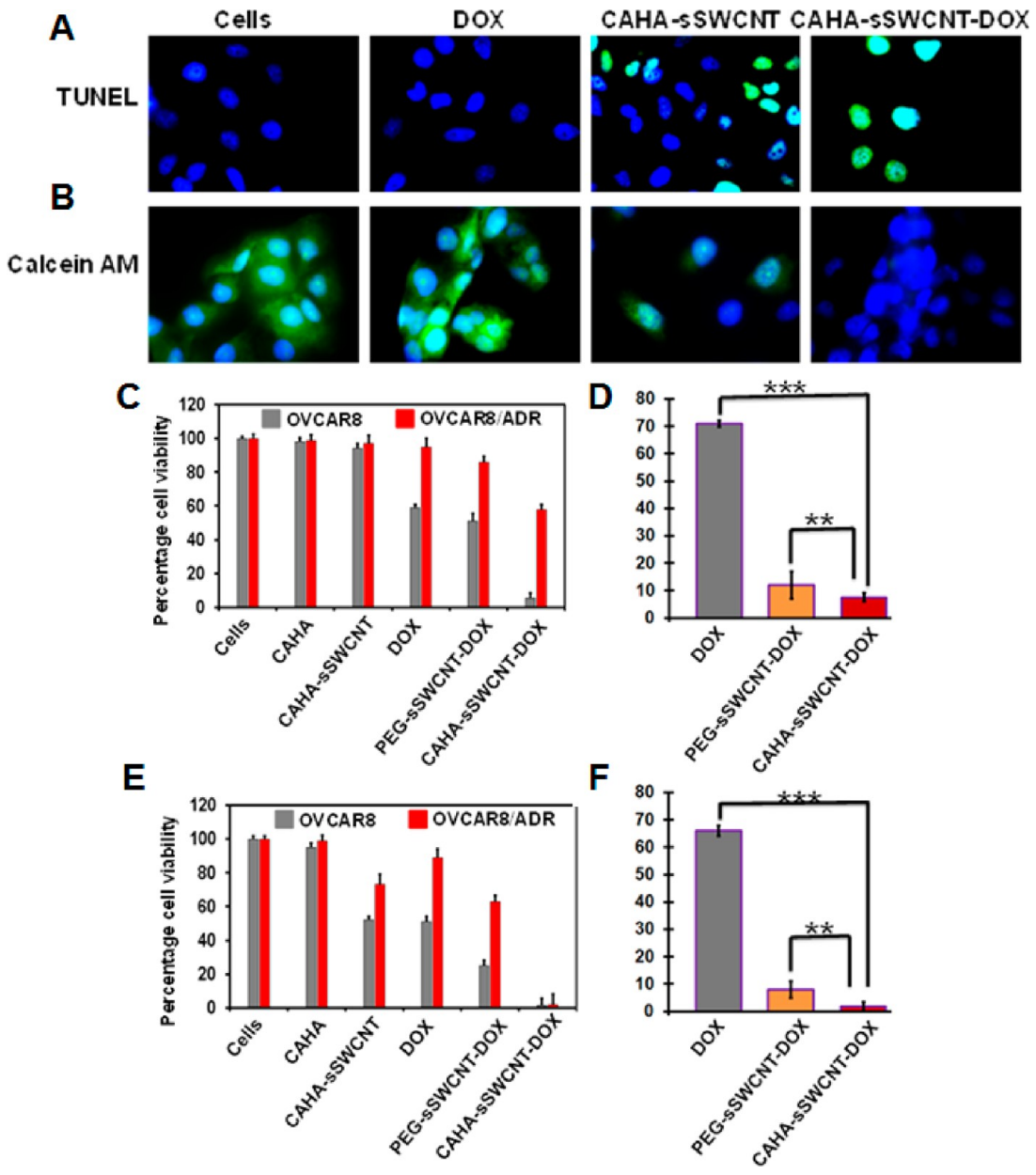

Figure 7. Drug-resistant cell treatment by CD44-targeted sSWCNT drug delivery and NIR laser irradiation. (A, B) OVCAR8/ADR cells were treated with free DOX or CAHA-sSWCNT-DOX and assessed for apoptosis (broken DNA fragments are labeled green) and cell membrane integrity (intact cell membranes are labeled green) using (A) TUNEL (apoptosis) and (B) Calcein AM (live cell) assays. Cells were treated with free DOX, CAHA-sSWCNTs, or CAHA-sSWCNT-DOX for 6 h and then irradiated with an 808 nm NIR laser probe at 0.5 W/cm^2 for 2.5 min. Cells were further incubated for 48 h and then fixed and stained for apoptosis with the TUNEL assay and for live cells using the Calcein AM assay. Green indicates positive for the assays, with cell nuclei stained blue using DAPI. (C−F) Percentage of viable cells after exposure to CAHA, CAHA-sSWCNTs, free DOX, PEG-sSWCNT-DOX, or CAHA-sSWCNT-DOX (DOX concentration adjusted to IC_{50} values of free DOX (OVCAR8 ∼2.1 μM and OVCAR8/ADR ∼150 μM without irradiation and OVCAR8 ∼1.5 μM and OVCAR8/ADR ∼100 μM with irradiation). (C) Cell viability in the absence of NIR laser irradiation ([DOX] = 2.1 μM). CAHA and CAHA-sSWCNTs are not cytotoxic. (D) Resistance factor (RF) of CAHA-sSWCNT-DOX (∼7.6) compared to the free drug (∼71.1) calculated by taking ratios of respective IC_{50} values of drug-resistant and drug-sensitive cells. (E) Cell viability of cancer cells irradiated with an 808 nm laser at 1 W/cm^2 for 2.5 min ([DOX] = 1.5 μM). The photothermal and photodynamic effects of CAHA-sSWCNTs in addition to DOX treatment led to very effective killing of both OVCAR8 and OVCAR8/ADR cells by CAHA-sSWCNT-DOX. (F) RF of CAHA-sSWCNT-DOX (∼1.3) compared to the free drug (∼66.7). **, $p < 0.01$; ***, $p < 0.001$.

high cancer cell specificity, enhanced drug delivery, and long-term physiological stability necessary to transport chemotherapeutic agents to resistant cancer cells with minimal nonspecificity and cytotoxicity and overcome the rigid resistant barrier. NIR laser probing on the nanoformula can induce apoptotic temperature and deliver chemotherapeutics to drug-resistant cancer cells. Our study also suggests that the influence of nanoformulations on the viscoelastic nature of drug-resistant cells should be accounted for while

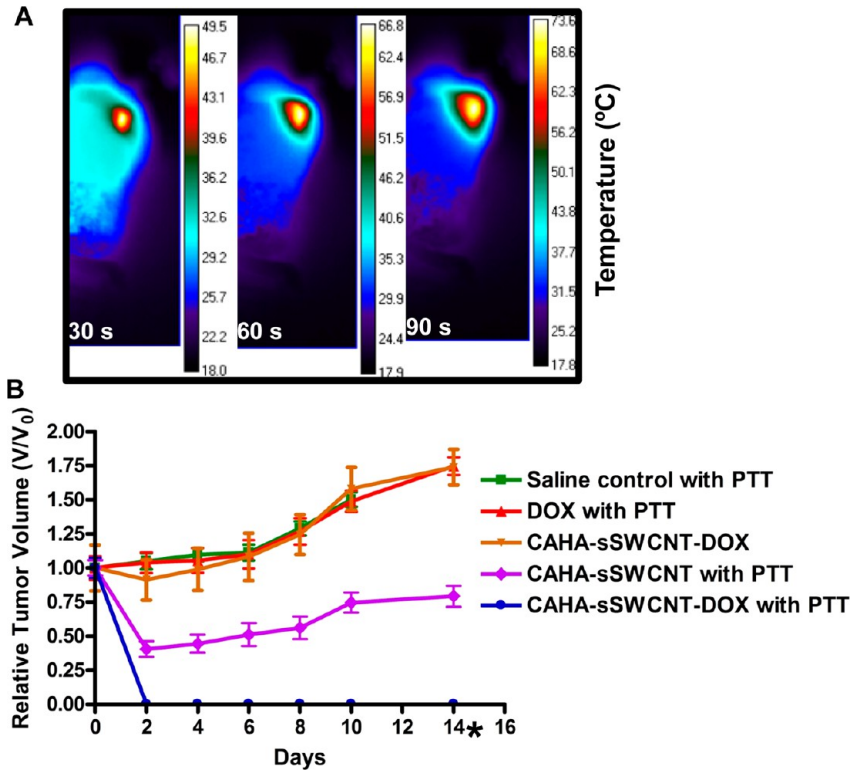

Figure 8. *In vivo* MDR tumor targeting by CD44-targeted CAHA-sSWCNT drug delivery and NIR irradiation system. (A) Thermal imaging of OVCAR8/ADR tumor xenograft exposed to an 808 NIR laser 24 h post CAHA-sSWCNT-DOX administration. (B) Eradication of pre-established OVCAR8/ADR MDR xenografts (n = 6/group) by a single CAHA-sSWCNT-DOX treatment (12 mg/kg DOX equivalent) followed by NIR laser irradiation (1 W/cm^2, 90 s).

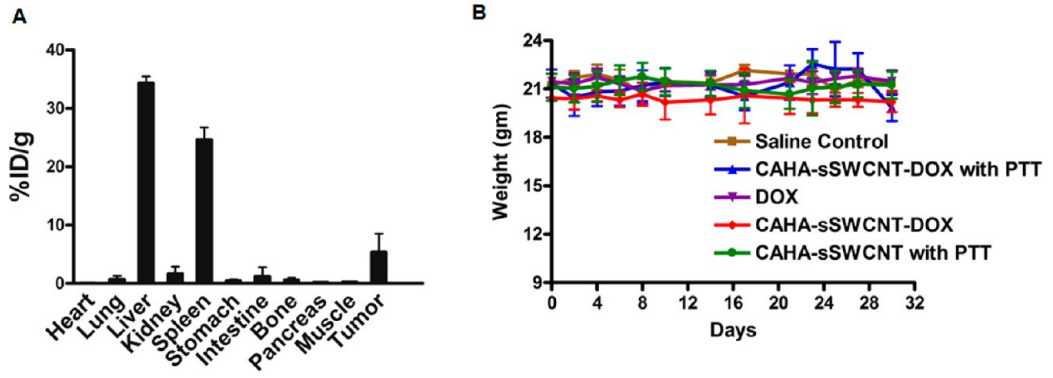

Figure 9. Biodistribution and body weight of SCID mice bearing OVCAR8/ADR tumor xenograft treated with CAHA-sSWCNT-DOX. (A) Raman spectroscopy quantification of the biodistribution of sSWCNTs. The histogram shows maximum accumulation of nanotubes in the liver and spleen followed by OVCAR8/ADR tumor. The other organs and tissues showed undetectable levels of the nanoparticles. (B) No apparent change in mouse body weight was observed over a period of 4 weeks after treatment with CAHA-sSWCNT-DOX and other formulas (n = 6/group).

formulating a targeted drug delivery system to overcome drug resistance. Our targeted drug delivery system, which delivers therapeutics and acts as a sensitizer to influence drug uptake and induce apoptosis, provides a novel effective means of counteracting the phenomenon of multidrug resistance.

MATERIALS AND METHODS

Synthesis of Nanoformulation. Synthesis of the sSWCNT dispersion involved simple sonication of the nanotubes in an aqueous solution of cholanic acid-derivatized hyaluronic acid.[36] Well-characterized and purified CAHA-sSWCNTs were loaded with either DOX through π stacking or imaging agents using EDC activation chemistry. The detailed synthesis procedure and characterization of the nanoformula are given in the Supporting Information. DOX loading was confirmed using UV−vis absorption spectroscopy.

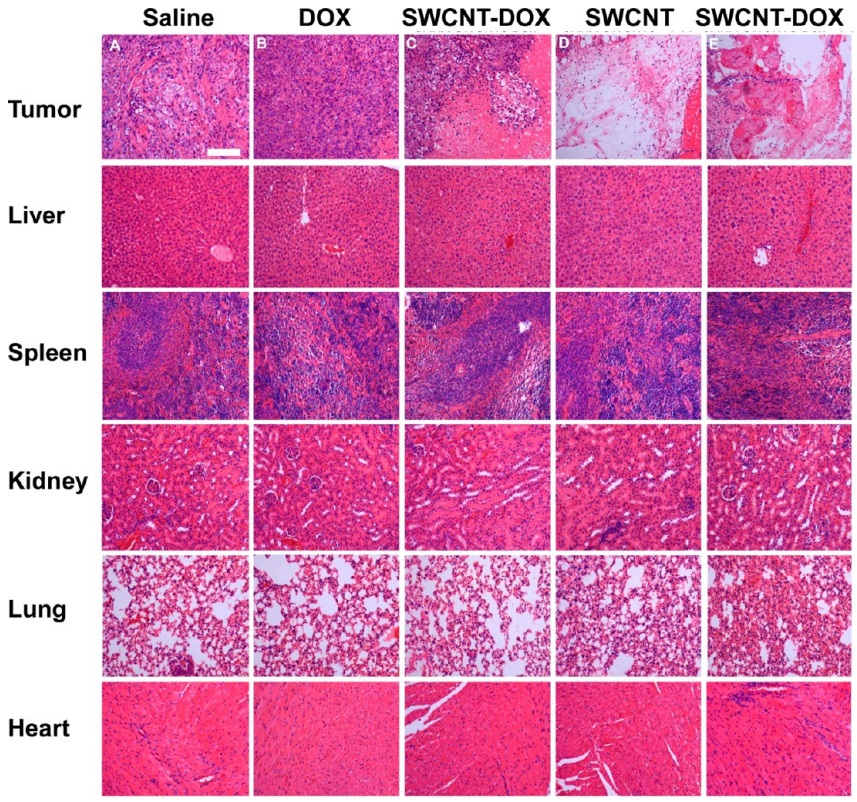

Figure 10. Histology of tumor mice treated with CAHA-sSWCNT-DOX. Hematoxylin and eosin (H&E) staining of tumors and primary organs of OVCAR8/ADR tumor xenograft bearing mice treated with CAHA-sSWCNT-DOX along with controls and exposed to 808 nm NIR irradiation 24 h post-treatment. (A) Saline with PTT, (B) free DOX with PTT, (C) CAHA-sSWCNT-DOX without PTT, (D) CAHA-sSWCNTs alone with PTT, and (E) CAHA-sSWCNT-DOX with PTT. Scale bar = 10 μm.

Cell Culture. We thank Dr. N. Neamati at the University of Southern California for providing OVCAR8 and OVCAR8/ADR cells. OVCAR8 and OVCAR8/ADR cancer cells were cultured in RPMI-1640 (Invitrogen) supplemented with 10% fetal bovine serum (FBS) at 37 °C in 95% air/5% CO_2. SCC7 (squamous cell carcinoma) and NIH3T3 mouse fibroblast cells were obtained from the American Type Culture Collection (Manassas, VA, USA). SCC7 cells were kept at 37 °C and 5% CO_2 in RPMI-1640 supplemented with 10% FBS, while NIH3T3 cells were incubated in DMEM medium (Cellgro) supplemented with 10% FBS. Freshly plated cells were grown overnight, to 50−70% confluency, prior to incubation with nanoformulations for imaging or therapeutic studies.

Confocal Imaging. OVCAR8 and OVCAR8/ADR ovarian cancer cells were grown to 50−60% confluency on an eight-well chambered LabTek II coverglass, treated with appropriately labeled dye-conjugate, and incubated for 6 h. Cells were washed with PBS three times and resuspended in fresh media. Live cell imaging was performed using an inverted Zeiss LSM 700 confocal microscope equipped with a CO_2 module, heating unit, and heating plate using a 40×/0.75 M27 EC Plan-Neofluar objective. Imaging was carried out at 37 °C in 5% CO_2 with cells plated in a LabTek II coverglass. Images were acquired and processed with the Zeiss Zen 2009 image software. The fluorescence micrographs shown are representative of at least three independent experiments. Average fluorescence intensity was quantified using Zen 2009 software.

Transmission Electron Microscope (TEM) Measurement. A specimen of CAHA-sSWCNTs for TEM imaging was prepared by depositing a 3 μL droplet from the aqueous solution onto a Quantifoil grid and left to dry in air. After adsorption for 3 min, the excess solution was blotted with filter paper, washed with a few 3 μL droplets of deionized water to remove any dirt, and left to dry. Images were recorded on a Tecnai TF30 TEM (FEI, Hillsboro, OR, USA) equipped with a GatanUltrascan 1000 CCD camera (Gatan, Pleasanton, CA, USA).

Raman Characterization. Raman characterization was used for the analysis of purity of CAHA-SWCNT samples for specific signature peaks. Raman characterization for obtaining the Raman profile of aqueous dispersed sSWCNT was done by using characteristic Raman signature peaks (G and D bands) of sSWCNTs. Raman spectra were recorded on a BWTek iRaman 785 spectrometer equipped with a microscope attachment, and the laser spot size was focused to 1 μm diameter (100× objective) and with a power output of 35 mW. The excitation source was an argon ion laser, 785 nm.

UV−Vis Absorption Measurement. CAHA-sSWCNT dispersion concentration was estimated using a UV−vis spectrophotometer (Thermo Scientific, Waltham, MA, USA), and a calibration curve by UV−vis absorbance was performed on samples with known concentrations. Absorbance at 808 nm was used as a marker for the concentration of CAHA-sSWCNTs.

Zeta Potential Measurement. To find the surface charge of CAHA, CAHA-sSWCNTs, and PEG-SWCNTs, zeta potential analysis was carried out using a Zetasizer Nano series (Zen3600) from Malvern with Zetasizer 6.0 software as the interface.

TUNEL Cell Death Assay. The APO-BrdU TUNEL (terminal transferased UTP nick end labeling) assay kit (Invitrogen) was used to detect cells undergoing apoptosis. Briefly, cells were grown onto eight-well chambered cell culture slides to 50−60% confluence, followed by treatment with CAHA-sSWCNTs, DOX, CAHA-sSWCNT-DOX, CAHA-sSWCNTs + DOX, and control cells alone. After treatment, the cells were washed in PBS (3× for x 2 min each) and incubated in fresh media for 1 h. Next, cells were fixed in 3.5% PBS−formaldehyde for 15 min at RT, rinsed in PBS (3×), and permeabilized in 0.5% PBS−Tween 20 for 5 min at RT followed by DNA end labeling for 1 h at 37 °C. Labeled cells were washed and incubated further with 95 μL of antibody staining solution (AlexaFluor 488-conjugated anti-BrdU) for 30 min at 37 °C, followed by additional washes (3×). Fluorescence image acquisitions were performed with Axio Plan 2 (Carl Zeiss).

MTT Assay. Cells were grown to 50−60% confluency overnight in 96-well plates. Media was aspirated, and the cells were incubated with fresh media containing either CAHA-sSWCNTs or sSWCNTs or CAHA at various concentrations along with control cells for 48 h. After treatment the cells were washed two times in PBS, and cells were incubated for an additional 24 h in fresh media. MTT was assessed using the CellTiter 96 AQ One Solution cell proliferation assay kit (Promega, MI, USA) and measured optically at 570 nm.

Calcein AM Cell Viability Assay. Cells (10^4 cells per well) were seeded in eight-well LabTek slides and incubated overnight. Then the cells were treated with nanotube formulations along with controls. Cells were washed with PBS 6 h post-treatment and incubated with 2 μM Calcein AM and 4 μM EthD-1 for 20 min at 37 °C. Then the cells were observed by fluorescence microscope.

Epifluorescence Imaging. An epifluorescence microscope was used to assess the presence of FITC conjugated onto the CAHA-SWCNTs in four different cell lines with varying CD44 expressions. For this, cells were treated with FITC-CAHA-sSWCNTs, washed, fixed, and stained with DAPI containing mounting media, and the images were acquired using a PerkinElmer LS55 fluorescence spectrometer.

Thermal Camera Measurement of Temperature. OVCAR8/ADR cells were grown to 60−70% confluency and then treated with the appropriate formula for 6 h. The cells were then washed and subjected to 808 nm NIR laser irradiation (LRD 808, Laserglow Technologies, CA, USA). The focus was adjusted to cover the entire well. The thermal camera (FLIR SC305, FLIR Systems, Inc., MA, USA) was pointed toward the well to record the change in temperature due to 808 nm laser irradiation. All the experiments were conducted at room temperature. The data obtained were later processed using ExaminIR MAX software.

FACS Analysis. For CD44 analysis, the cells were trypsinized, followed by washing three times with PBS, and finally suspended in FACS buffer (R&D, Inc.). Anti-CD44 primary antibody (clone IM7, BD Biosciences, NJ, USA) was diluted 1:100 with FACS buffer. The suspended cells in FACS buffer were centrifuged and resuspended in anti-CD44 containing FACS buffer, followed by incubation on ice for 1 h. Then, cells were centrifuged and washed four times with FACS buffer before incubation with the corresponding FITC-conjugated secondary antibody for 30 min. Then, the cells were centrifuged and washed four times in FACS buffer, and the cell surface CD44 expression level was measured by flow cytometry (BD Accuri C6 flow cytometer).

High-Resolution Biological AFM. Biological AFM imaging of the sSWCNTs with CAHA was performed in air using gentle-tapping-mode AFM, mostly with a PicoForce Multimode AFM (Bruker, CA, USA) consisting of a Nanoscope V controller, a type E scanner head, and a sharpened FESP-SS (Bruker) or similar AFM cantilever. For CAHA-sSWCNT visualization, suitable attachment was readily achieved by a 30 min incubation of the sample in deionized water on freshly peeled mica substrates, followed by rinsing with deionized water (4×) and complete drying under an inert N_2 gas flow. The sample was then sealed into the instrument compartment dehumidified by Drierite particles. AFM images were evaluated with the Nanoscope software (version 7.3, Bruker) and exported to NIH ImageJ (version 1.41o) for further analyses and display.

Quartz-Crystal Microbalance with Dissipation Measurement. A quartz-crystal microbalance with dissipation instrument (QCM-D E1, Biolin Scientific/Q-Sense, MD, USA) was used to record changes in energy dissipation (ΔD) and resonant frequency (ΔF) as a function of time. All measurements were done with optically polished gold deposited quartz crystals (AT-cut, 14 mm disks) with a fundamental resonant frequency of 5 MHz (QSX 301). The sensors were prepared as follows: QCM-D sensors were cleaned using a UV/ozone cleaner for 10 min. The sensors were then dipped in a mixture of 10 mL of pure water, 2 mL of ammonium hydroxide, and 2 mL of hydrogen peroxide at 75 °C for 5 min. Then the sensors were rinsed with pure water and sonicated for 2 min. Later, cleaned sensors were dried using a gentle stream of nitrogen. The cleaned sensors were then dipped in 5 mM 3-mercaptopropionic acid (3-MPA) overnight. 3-MPA-modified sensors were rinsed in ethanol and pure water thoroughly and incubated with polylysine for 1 h. Then the sensors were rinsed with water, dried, and used for culturing the cells. Then 100 μL of 1.5 × 105 OVCAR8 cells and OVCAR8/ADR cells were incubated with the sensors in a humidified atmosphere at 37 °C and 5% CO_2. After reaching 90% confluency, the cells were washed using assay buffer (20 mM HEPES buffer, pH 7.2), and the back of the sensor was wiped gently with a Kimwipe to remove the residual buffer. The sensor was then mounted in a flow module (Q sense), and the assay buffer at 37 °C was injected. Once the assay buffer was exited through the outlet of the flow module, the flow stopped and the changes in frequency (ΔF) and dissipation (ΔD) were recorded simultaneously. After obtaining the stable baselines, flow was resumed by changing the tube to CAHA-sSWCNTs or just CAHA solutions that were prewarmed to 37 °C. Flow stopped once the CAHA-sSWCNT/CAHA solutions completely filled the sensor chamber and came through the outlet of the flow module. Changes in frequency and dissipation were recorded simultaneously at 37 °C for 1 h.

Animal Protocol. All animal operations were in accordance with institutional animal use and care regulations. OVCAR8/ADR tumor-bearing mice were prepared by subcutaneously injecting a suspension of 1×10^7 OVCAR8/ADR cells in PBS (100 μL) into bilateral shoulders of female SCID mice (6 weeks old, 20−25 g). When the tumor size reached ∼60 mm^3, all the tumor-bearing mice were randomly divided into five groups (n = 6 per group): group 1, saline control; group 2, free DOX (12 mg/kg); group 3, CAHA-sSWCNT-DOX; group 4, CAHA-sSWCNTs (100 μg/mL, 100 μL); group 5, CAHA-sSWCNT-DOX (DOX dose ∼12 mg/kg) without laser. All groups were exposed to NIR laser irradiation except for group 5. For groups with laser treatment, at 24 h postinjection, each mouse was anesthetized using isoflurane and exposed to an 808 nm laser at a power density of 1 W/cm^2 for 90 s. After the irradiation, the tumor regrowth of each mouse was monitored. The tumor size was measured by caliper every 2 days after treatment. Tumor volume (V) was determined by the following equation: $V = AB^2/2$, where A is the longer and B is the shorter diameter (mm). The relative tumor volumes were normalized to their initial sizes. During the treatment, thermal imaging was recorded by an SC300 infrared camera (FLIR). The animals were monitored for 30 days to investigate the phenotypical response. During this period, physical examinations including weights and behaviors were performed regularly. At the end of the study period, the mice were euthanized and necropsy was performed to harvest the major organs (*i.e.*, spleen, liver, kidney, heart, and lung). These organs were fixed and stained with H&E for histology study.

Histological Staining. Major organs were collected from the euthanized OVCAR8/ADR tumor bearing mice at 24 h post-PTT. Tissues were fixed in a 4% formaldehyde solution at room temperature for at least 48 h. H&E staining (BBC Biochemical, Mount Vernon, WA, USA) was performed and observed with a BX41 bright field microscopy (Olympus).

Statistical Analysis. Statistical analyses were conducted with Prism 4.0 software (GraphPad Inc. San Diego, CA, USA). Results were expressed as mean and SD. Two-tailed paired and unpaired Student's t tests were used to determine differences within groups and between groups, respectively. $p < 0.05$ was regarded as statistically significant.

Conflict of Interest: The authors declare no competing financial interest.

Acknowledgment. This work was supported in part by an NRC NIST/NIH fellowship and by the Intramural Research Program (IRP) of the National Institute of Biomedical Imaging and Bioengineering (NIBIB), National Institutes of Health (NIH). We also thank Dr. Paul Smith for his laser work, Dr. Alioscka Sousa for his TEM work, and Mrs. Rohini Bhirde for illustrations.

Supporting Information Available: Details of synthesis and characterization of CAHA-coated and drug-loaded semiconducting single-walled carbon nanotubes can be found in the Supporting Information. This material is available free of charge *via* the Internet at http://pubs.acs.org.

REFERENCES AND NOTES

1. Gottesman, M. M.; Fojo, T.; Bates, S. E. Multidrug Resistance in Cancer: Role of ATP-Dependent Transporters. *Nat. Rev. Cancer* **2002**, *2*, 48–58.
2. Szakacs, G.; Paterson, J. K.; Ludwig, J. A.; Booth-Genthe, C.; Gottesman, M. M. Targeting Multidrug Resistance in Cancer. *Nat. Rev. Drug Discovery* **2006**, *5*, 219–234.
3. Luqmani, Y. A. Mechanisms of Drug Resistance in Cancer Chemotherapy. *Med. Princ. Pract.* **2005**, *14*), 35–48.
4. Weis, S. M.; Cheresh, D. A. Tumor Angiogenesis: Molecular Pathways and Therapeutic Targets. *Nat. Med.* **2011**, *17*, 1359–1370.
5. Thigpen, T. A Rational Approach to the Management of Recurrent or Persistent Ovarian Carcinoma. *Clin. Obstet. Gynecol.* **2012**, *55*, 114–130.
6. Patel, A. G.; Kaufmann, S. H. How Does Doxorubicin Work? *eLife* **2012**, *1*, e00387.
7. Broxterman, H. J.; Gotink, K. J.; Verheul, H. M. Understanding the Causes of Multidrug Resistance in Cancer: A Comparison of Doxorubicin and Sunitinib. *Drug Resist. Updates* **2009**, *12*, 114–126.
8. Huang, H. C.; Yang, Y.; Nanda, A.; Koria, P.; Rege, K. Synergistic Administration of Photothermal Therapy and Chemotherapy to Cancer Cells Using Polypeptide-Based Degradable Plasmonic Matrices. *Nanomedicine (London, U.K.)* **2011**, *6*, 459–473.
9. Miletti-Gonzalez, K. E.; Chen, S.; Muthukumaran, N.; Saglimbeni, G. N.; Wu, X.; Yang, J.; Apolito, K.; Shih, W. J.; Hait, W. N.; Rodriguez-Rodriguez, L. The CD44 Receptor Interacts with P-Glycoprotein to Promote Cell Migration and Invasion in Cancer. *Cancer Res.* **2005**, *65*, 6660–6667.
10. Zoller, M. CD44: Can a Cancer-Initiating Cell Profit from an Abundantly Expressed Molecule? *Nat. Rev. Cancer* **2011**, *11*, 254–267.
11. Ponta, H.; Sherman, L.; Herrlich, P. A. CD44: From Adhesion Molecules to Signalling Regulators. *Nat. Rev. Mol. Cell Biol.* **2003**, *4*, 33–45.
12. Cain, J. W.; Hauptschein, R. S.; Stewart, J. K.; Bagci, T.; Sahagian, G. G.; Jay, D. G. Identification of CD44 as a Surface Biomarker for Drug Resistance by Surface Proteome Signature Technology. *Mol. Cancer Res.* **2011**, *9*, 637–647.
13. Casagrande, F.; Cocco, E.; Bellone, S.; Richter, C. E.; Bellone, M.; Todeschini, P.; Siegel, E.; Varughese, J.; Arin-Silasi, D.; Azodi, M.; *et al*. Eradication of Chemotherapy-Resistant CD44+ Human Ovarian Cancer Stem Cells in Mice by Intraperitoneal Administration of Clostridium Perfringens Enterotoxin. *Cancer* **2011**, *117*, 5519–5528.
14. Eliaz, R. E.; Szoka, F. C., Jr. Liposome-Encapsulated Doxorubicin Targeted to CD44: A Strategy to Kill CD44-Overexpressing Tumor Cells. *Cancer Res.* **2001**, *61*, 2592–2601.
15. Peer, D.; Karp, J. M.; Hong, S.; Farokhzad, O. C.; Margalit, R.; Langer, R. Nanocarriers as an Emerging Platform for Cancer Therapy. *Nat. Nanotechnol.* **2007**, *2*, 751–760.
16. Wagner, V.; Dullaart, A.; Bock, A. K.; Zweck, A. The Emerging Nanomedicine Landscape. *Nat. Biotechnol.* **2006**, *24*, 1211–1217.
17. Chen, W.; Xu, N.; Xu, L.; Wang, L.; Li, Z.; Ma, W.; Zhu, Y.; Xu, C.; Kotov, N. A. Multifunctional Magnetoplasmonic Nanoparticle Assemblies for Cancer Therapy and Diagnostics (Theranostics). *Macromol. Rapid Commun.* **2010**, *31*, 228–236.
18. Pelaz, B.; Jaber, S.; de Aberasturi, D. J.; Wulf, V.; Aida, T.; de la Fuente, J. M.; Feldmann, J.; Gaub, H. E.; Josephson, L.; Kagan, C. R.; *et al*. The State of Nanoparticle-Based Nanoscience and Biotechnology: Progress, Promises, and Challenges. *ACS Nano* **2012**, *6*, 8468–8483.
19. Ferrari, M. Cancer Nanotechnology: Opportunities and Challenges. *Nat. Rev. Cancer* **2005**, *5*, 161–171.
20. Bhirde, A. A.; Kapoor, A.; Liu, G.; Iglesias-Bartolome, R.; Jin, A.; Zhang, G.; Xing, R.; Lee, S.; Leapman, R. D.; Gutkind, J. S.; *et al*. Nuclear Mapping of Nanodrug Delivery Systems in Dynamic Cellular Environments. *ACS Nano* **2012**, *6*, 4966–4972.
21. Reungwetwattana, T.; Eadens, M. J.; Molina, J. R. Chemotherapy for Non-Small-Cell Lung Carcinoma: From a Blanket Approach to Individual Therapy. *Semin. Respir. Crit. Care Med.* **2011**, *32*, 78–93.
22. Bhirde, A. A.; Patel, V.; Gavard, J.; Zhang, G.; Sousa, A. A.; Masedunskas, A.; Leapman, R. D.; Weigert, R.; Gutkind, J. S.; Rusling, J. F. Targeted Killing of Cancer Cells *in Vivo* and *in Vitro* with EGF-Directed Carbon Nanotube-Based Drug Delivery. *ACS Nano* **2009**, *3*, 307–316.
23. Gao, J.; Feng, S. S.; Guo, Y. Nanomedicine against Multidrug Resistance in Cancer Treatment. *Nanomedicine (London, U.K.)* **2012**, *7*, 465–468.
24. Shapira, A.; Livney, Y. D.; Broxterman, H. J.; Assaraf, Y. G. Nanomedicine for Targeted Cancer Therapy: Towards the Overcoming of Drug Resistance. *Drug Resist. Updates* **2011**, *14*, 150–163.
25. Gao, Z.; Zhang, L.; Sun, Y. Nanotechnology Applied to Overcome Tumor Drug Resistance. *J. Controlled Release* **2012**, *162*, 45–55.
26. Kievit, F. M.; Wang, F. Y.; Fang, C.; Mok, H.; Wang, K.; Silber, J. R.; Ellenbogen, R. G.; Zhang, M. Doxorubicin Loaded Iron Oxide Nanoparticles Overcome Multidrug Resistance in Cancer *in Vitro*. *J. Controlled Release* **2011**, *152*, 76–83.
27. Bianco, A.; Kostarelos, K.; Prato, M. Opportunities and Challenges of Carbon-Based Nanomaterials for Cancer Therapy. *Expert Opin. Drug Delivery* **2008**, *5*, 331–342.
28. Kostarelos, K.; Bianco, A.; Prato, M. Promises, Facts and Challenges for Carbon Nanotubes in Imaging and Therapeutics. *Nat. Nanotechnol.* **2009**, *4*, 627–633.
29. Liu, Z.; Tabakman, S.; Welsher, K.; Dai, H. Carbon Nanotubes in Biology and Medicine: In Vitro and in Vivo Detection, Imaging and Drug Delivery. *Nano Res.* **2009**, *2*, 85–120.
30. Liu, Z.; Cai, W.; He, L.; Nakayama, N.; Chen, K.; Sun, X.; Chen, X.; Dai, H. *In Vivo* Biodistribution and Highly Efficient Tumour Targeting of Carbon Nanotubes in Mice. *Nat. Nanotechnol.* **2007**, *2*, 47–52.
31. Liu, Z.; Chen, K.; Davis, C.; Sherlock, S.; Cao, Q.; Chen, X.; Dai, H. Drug Delivery with Carbon Nanotubes for *in Vivo* Cancer Treatment. *Cancer Res.* **2008**, *68*, 6652–6660.
32. Liu, Z.; Fan, A. C.; Rakhra, K.; Sherlock, S.; Goodwin, A.; Chen, X.; Yang, Q.; Felsher, D. W.; Dai, H. Supramolecular Stacking of Doxorubicin on Carbon Nanotubes for *in Vivo* Cancer Therapy. *Angew. Chem., Int. Ed.* **2009**, *48*, 7668–7672.
33. Bhirde, A. A.; Patel, S.; Sousa, A. A.; Patel, V.; Molinolo, A. A.; Ji, Y.; Leapman, R. D.; Gutkind, J. S.; Rusling, J. F. Distribution and Clearance of PEG-Single-Walled Carbon Nanotube Cancer Drug Delivery Vehicles in Mice. *Nanomedicine (London, U.K.)* **2010**, *5*, 1535–1546.
34. Simmons, T. J.; Bult, J.; Hashim, D. P.; Linhardt, R. J.; Ajayan, P. M. Noncovalent Functionalization as an Alternative to Oxidative Acid Treatment of Single Wall Carbon Nanotubes with Applications for Polymer Composites. *ACS Nano* **2009**, *3*, 865–870.
35. Liang, S.; Zhao, Y.; Adronov, A. Selective and Reversible Noncovalent Functionalization of Single-Walled Carbon Nanotubes by a pH-Responsive Vinylogous Tetrathiafulvalene-Fluorene Copolymer. *J. Am. Chem. Soc.* **2014**, *136*, 970–977.
36. Swierczewska, M.; Choi, K. Y.; Mertz, E. L.; Huang, X.; Zhang, F.; Zhu, L.; Yoon, H. Y.; Park, J. H.; Bhirde, A.; Lee, S.; *et al*. A Facile, One-Step Nanocarbon Functionalization for Biomedical Applications. *Nano Lett.* **2012**, *12*, 3613–3620.
37. Rutherglen, C.; Jain, D.; Burke, P. Nanotube Electronics for Radiofrequency Applications. *Nat. Nanotechnol.* **2009**, *4*, 811–819.
38. Krauss, T. D. Biosensors: Nanotubes Light Up Cells. *Nat. Nanotechnol.* **2009**, *4*, 85–86.
39. Khan, I. A.; Afrooz, A. R.; Flora, J. R.; Schierz, P. A.; Ferguson, P. L.; Sabo-Attwood, T.; Saleh, N. B. Chirality Affects Aggregation Kinetics of Single-Walled Carbon Nanotubes. *Environ. Sci. Technol.* **2013**, *47*, 1844–1852.
40. Murakami, T.; Nakatsuji, H.; Inada, M.; Matoba, Y.; Umeyama, T.; Tsujimoto, M.; Isoda, S.; Hashida, M.; Imahori, H. Photodynamic and Photothermal Effects of Semiconducting and Metallic-Enriched Single-Walled Carbon Nanotubes. *J. Am. Chem. Soc.* **2012**, *134*, 17862–17865.
41. Antaris, A. L.; Robinson, J. T.; Yaghi, O. K.; Hong, G.; Diao, S.; Luong, R.; Dai, H. Ultra-Low Doses of Chirality Sorted (6,5) Carbon Nanotubes for Simultaneous Tumor Imaging and Photothermal Therapy. *ACS Nano* **2013**, *7*, 3644–3652.

42. Chen, S. S.; Michael, A.; Butler-Manuel, S. A. Advances in the Treatment of Ovarian Cancer: A Potential Role of Antiinflammatory Phytochemicals. *Discovery Med.* **2012**, *13*, 7–17.
43. Yap, T. A.; Carden, C. P.; Kaye, S. B. Beyond Chemotherapy: Targeted Therapies in Ovarian Cancer. *Nat. Rev. Cancer* **2009**, *9*, 167–181.
44. Agarwal, R.; Kaye, S. B. Ovarian Cancer: Strategies for Overcoming Resistance to Chemotherapy. *Nat. Rev. Cancer* **2003**, *3*, 502–516.
45. Cheng, W.; Liu, T.; Wan, X.; Gao, Y.; Wang, H. MicroRNA-199a Targets CD44 to Suppress the Tumorigenicity and Multidrug Resistance of Ovarian Cancer-Initiating Cells. *FEBS J.* **2012**, *279*, 2047–2059.
46. Wei, X.; Dombkowski, D.; Meirelles, K.; Pieretti-Vanmarcke, R.; Szotek, P. P.; Chang, H. L.; Preffer, F. I.; Mueller, P. R.; Teixeira, J.; MacLaughlin, D. T.; *et al*. Mullerian Inhibiting Substance Preferentially Inhibits Stem/Progenitors in Human Ovarian Cancer Cell Lines Compared with Chemotherapeutics. *Proc. Natl. Acad. Sci. U.S.A.* **2010**, *107*, 18874–18879.
47. Toole, B. P. Hyaluronan: From Extracellular Glue to Pericellular Cue. *Nat. Rev. Cancer* **2004**, *4*, 528–539.
48. Toole, B. P. Hyaluronan-CD44 Interactions in Cancer: Paradoxes and Possibilities. *Clin. Cancer Res.* **2009**, *15*, 7462–7468.
49. Choi, K. Y.; Chung, H.; Min, K. H.; Yoon, H. Y.; Kim, K.; Park, J. H.; Kwon, I. C.; Jeong, S. Y. Self-Assembled Hyaluronic Acid Nanoparticles for Active Tumor Targeting. *Biomaterials* **2010**, *31*, 106–114.
50. Choi, K. Y.; Yoon, H. Y.; Kim, J. H.; Bae, S. M.; Park, R. W.; Kang, Y. M.; Kim, I. S.; Kwon, I. C.; Choi, K.; Jeong, S. Y.; *et al*. Smart Nanocarrier Based on PEGylated Hyaluronic Acid for Cancer Therapy. *ACS Nano* **2011**, *5*, 8591–8599.
51. Zhou, F.; Xing, D.; Wu, B.; Wu, S.; Ou, Z.; Chen, W. R. New Insights of Transmembranal Mechanism and Subcellular Localization of Noncovalently Modified Single-Walled Carbon Nanotubes. *Nano Lett.* **2010**, *10*, 1677–1681.
52. Robinson, J. T.; Welsher, K.; Tabakman, S. M.; Sherlock, S. P.; Wang, H.; Luong, R.; Dai, H. High Performance in Vivo Near-IR (>1 mum) Imaging and Photothermal Cancer Therapy with Carbon Nanotubes. *Nano Res.* **2010**, *3*, 779–793.
53. Xiao, Y.; Gao, X.; Taratula, O.; Treado, S.; Urbas, A.; Holbrook, R. D.; Cavicchi, R. E.; Avedisian, C. T.; Mitra, S.; Savla, R.; *et al*. Anti-HER2 IgY Antibody-Functionalized Single-Walled Carbon Nanotubes for Detection and Selective Destruction of Breast Cancer Cells. *BMC Cancer* **2009**, *9*, 351.
54. Tang, Y.; McGoron, A. J. Combined Effects of Laser-ICG Photothermotherapy and Doxorubicin Chemotherapy on Ovarian Cancer Cells. *J. Photochem. Photobiol. B* **2009**, *97*, 138–144.
55. Hudson, D. E.; Hudson, D. O.; Wininger, J. M.; Richardson, B. D. Penetration of Laser Light at 808 and 980 nm in Bovine Tissue Samples. *Photomed. Laser Surg.* **2013**, *31*, 163–168.
56. Tu, X.; Manohar, S.; Jagota, A.; Zheng, M. DNA Sequence Motifs for Structure-Specific Recognition and Separation of Carbon Nanotubes. *Nature* **2009**, *460*, 250–253.
57. Lorenzi, P. L.; Reinhold, W. C.; Varma, S.; Hutchinson, A. A.; Pommier, Y.; Chanock, S. J.; Weinstein, J. N. DNA Fingerprinting of the NCI-60 Cell Line Panel. *Mol. Cancer Ther.* **2009**, *8*, 713–24.
58. Cho, N. J.; Frank, C. W.; Kasemo, B.; Hook, F. Quartz Crystal Microbalance with Dissipation Monitoring of Supported Lipid Bilayers on Various Substrates. *Nat. Protoc.* **2010**, *5*, 1096–1106.
59. Chen, J. Y.; Shahid, A.; Garcia, M. P.; Penn, L. S.; Xi, J. Dissipation Monitoring for Assessing EGF-Induced Changes of Cell Adhesion. *Biosens. Bioelectron.* **2012**, *38*, 375–381.
60. Cross, S. E.; Jin, Y. S.; Rao, J.; Gimzewski, J. K. Nanomechanical Analysis of Cells from Cancer Patients. *Nat. Nanotechnol.* **2007**, *2*, 780–783.
61. Liu, Z.; Davis, C.; Cai, W.; He, L.; Chen, X.; Dai, H. Circulation and Long-Term Fate of Functionalized, Biocompatible Single-Walled Carbon Nanotubes in Mice Probed by Raman Spectroscopy. *Proc. Natl. Acad. Sci. U.S.A.* **2008**, *105*, 1410–1415.
62. Mizrahy, S.; Raz, S. R.; Hasgaard, M.; Liu, H.; Soffer-Tsur, N.; Cohen, K.; Dvash, R.; Landsman-Milo, D.; Bremer, M. G.; Moghimi, S. M.; *et al*. Hyaluronan-Coated Nanoparticles: The Influence of the Molecular Weight on CD44-Hyaluronan Interactions and on the Immune Response. *J. Controlled Release* **2011**, *156*, 231–238.
63. Cohen, K.; Emmanuel, R.; Kisin-Finfer, E.; Shabat, D.; Peer, D. Modulation of Drug Resistance in Ovarian Adenocarcinoma Using Chemotherapy Entrapped in Hyaluronan-Grafted Nanoparticle Clusters. *ACS Nano* **2014**, *8*, 2183–2195.
64. Liu, Z.; Sun, X.; Nakayama-Ratchford, N.; Dai, H. Supramolecular Chemistry on Water-Soluble Carbon Nanotubes for Drug Loading and Delivery. *ACS Nano* **2007**, *1*, 50–56.